

Microstructure of shear-thickening concentrated suspensions determined by flow-USANS

Dennis P. Kalman · Norman J. Wagner

Received: 6 December 2008 / Accepted: 22 February 2009 / Published online: 28 March 2009
© Springer-Verlag 2009

Abstract Reversible shear thickening in colloidal suspensions is a consequence of the formation of hydroclusters due to the dominance of short-ranged lubrication hydrodynamic interactions at relatively high shear rates. Here, we develop and demonstrate a new method of flow-ultra small angle neutron scattering to probe the colloidal microstructure under steady flow conditions on length scales suitable to characterize the formation of hydroclusters. Results are presented for a model near hard-sphere colloidal suspension of 260 nm radius (10% polydisperse) sterically stabilized silica particles in poly(ethylene glycol) at shear rates in the shear thinning and shear thickening regime for dilute, moderately concentrated, and concentrated (ordered) suspensions. Hydrocluster formation is observed as correlated, broadly distributed density fluctuations in the suspension with a characteristic length scale of a few particle diameters. An order–disorder transition is observed to be coincident with shear thickening for the most concentrated sample, but the shear-thickened state shows hydrocluster formation. These structural observations are correlated to the behavior of the shear viscosity and discussed within the framework of theory, simulation, and prior experiments.

Keywords Suspensions · Colloids · Shear-thickening · Microstructure · Hydrocluster

Paper presented at Workshop on Rheophysics on January 7–9, 2008, in Paris, France.

D. P. Kalman · N. J. Wagner (✉)
Department of Chemical Engineering,
University of Delaware,
Newark, DE 19716, USA
e-mail: wagnernj@udel.edu

Introduction

The nonlinear rheology of colloidal dispersions is a direct response of flow-induced microstructural rearrangements. One of the most significant changes evident in stable, colloidal dispersion is shear thickening (Barnes 1989), which is ubiquitous and marked by a shear viscosity that increases with increasing applied shear rate or shear stress. Shear thickening plagues processes with high shear rates and high particle concentrations, such as paper coating, spraying, and the efficient pumping of slurries, as well as the use of concrete (Lootens et al. 2004). However, it can be harnessed for benefit in novel electrorheological fluids (Shenoy et al. 2003), unique materials that can simultaneously stiffen and dampen (Fischer et al. 2007), stab, and puncture resistant flexible composites (Decker et al. 2007), as well as enhanced body armor (Lee et al. 2003). Shear thickening has been shown to be a very sensitive probe of the nanoscale forces operational in controlling dense suspension rheology (Wagner and Bender 2004).

The mechanism for reversible shear thickening in stable colloidal dispersions is understood to be driven by the dominance of short-range lubrication hydrodynamic interactions, which lead to particle clustering (Brady and Bossis 1985). These flow-induced particle density fluctuations, denoted as “hydroclusters,” first predicted by Stokesian dynamics simulations, were then observed experimentally by rheo-optical (Bender and Wagner 1995; Dhaene et al. 1993) and neutron scattering methods (Bender and Wagner 1996; Maranzano and Wagner 2002; Newstein et al. 1999). A fundamental theoretical understanding of hydrocluster formation has been developed via suspension micromechanics

(Bergenholtz et al. 2002; Brady and Morris 1997). Understanding the formation and structure of these hydroclusters is fundamental to understanding suspension rheology (Brady 1996). As noted by Brady and Bossis in their seminal review of the Stokesian dynamics method (Brady and Bossis 1988): “Thus the importance of cluster formation, which results from the lubrication forces and excluded volume, cannot be underestimated in understanding suspension behavior.”

Simultaneous measurements of structure and rheology are required to elucidate the mechanism by which flow-induced microstructural rearrangements manifest in nonlinear suspension rheology. Previous work has examined the structure of concentrated colloidal suspensions under shear flow via small angle neutron scattering (SANS) (Ackerson et al. 1986; Bender and Wagner 1996; Dekruif et al. 1988; Gopalakrishnan and Zukoski 2004; Johnson et al. 1988; Laun et al. 1992; Lee and Wagner 2006; Lindner and Oberthur 1984; Maranzano and Wagner 2002; Newstein et al. 1999; Vanderwerff et al. 1990; Watanabe et al. 1998), but SANS is limited to particle radii under 100 nm to be able to capture the structure on the nearest neighbor length scales and substantially smaller particles are required in order to probe longer length scale clustering. However, the stresses and, hence, shear rates required for the onset of shear thickening in hard sphere dispersions scale inversely with particle size cubed (Krishnamurthy et al. 2005; Lee and Wagner 2006; Maranzano and Wagner 2001), making it difficult to generate, as well as maintain, a stable experiment for sufficiently long durations at the required high shear rates in the SANS Couette cell (see, for example, Bender and Wagner 1996; O’Brien and Mackay 2000). Larger, $\sim 0.5\text{-}\mu\text{m}$ particles have been used in commercially relevant protective materials of recent interest; however, rheo-SANS experiments are unable to probe the length scales required to observe hydrocluster formation in these suspensions. Finally, although suitable length scales can be probed with light scattering (Ackerson et al. 1989; Tomita and Vandeven 1984; Wagner and Russel 1990; Woutersen et al. 1993) or direct visualization (Vermant and Solomon 2005), few concentrated dispersions are suitably transparent.

Small-angle X-ray scattering and ultra-small-angle X-ray scattering have also been employed to probe dilute and concentrated colloidal dispersions (Hoekstra et al. 2002, 2005; Versmold et al. 2001, 2002a, b, 2005) and could potentially achieve the length scales of interest here. However, X-ray scattering from concentrated suspensions can be limited by multiple scattering and background scattering, which cannot be easily mitigated in an X-ray scattering experiment. Isotope substi-

tution, however, can reduce unwanted background and multiple scattering in SANS experiments.

To probe hydrocluster formation in model hard-sphere dispersions, we develop a new method of flow-ultra small angle neutron scattering (USANS) to probe length scales up to 20 μm (Bhatia 2005) in a suspension under steady shear flow. Here, we report the first flow-USANS measurements on concentrated colloidal dispersions to examine the suspension microstructure and, in particular, the possible formation of hydroclusters in the shear thickening flows at high shear rates.

Experimental

Materials

Commercially sourced silica particles obtained as a dry powder were dispersed in poly(ethylene glycol) (PEG-200, Clariant, $\eta = 42\text{ mPa}\cdot\text{s}$) by roll mixing for 24 h at room temperature. The particle density was determined via solution densitometry (Anton Paar, Model DMA 48) in PEG-200 following a standard protocol (Lee and Wagner 2006) and the values are reported in Table 1. Dynamic light scattering (DLS) measurements (Brookhaven Zeta-PALS at 678.0 nm and 90°, five repeats on four samples of varying concentration in ethanol) yielded a hydrodynamic radius of $289 \pm 58\text{ nm}$ (errors given are 95% confidence intervals). Scanning electronic microscopy (SEM) images were analyzed by taking two perpendicular measures per particle on 22 particles from two micrographs (Fig. 1). This measurement yielded a number average radius of $255 \pm 20\text{ nm}$, and the measured particle aspect ratio was not statistically different from zero. As will be shown, a USANS measurement discussed below yields a fit particle size of 260 nm diameter with 10% polydispersity based on a Schulz distribution (Schulz et al. 1962; Wagner et al. 1991). The excellent agreement between the measurements shows the particles to

Table 1 System properties and data

ρ_{SiO_2}	1.96	g/mL
ρ_{PEG}	1.13	g/mL
η_{PEG}	42	mPa·s
Mobility	$< 10^{-11}$	$\text{m}^2\cdot\text{V}^{-1}\text{ s}^{-1}$
a —DLS	289 ± 58	nm
a —SEM	255 ± 20	nm
a —USANS	260 ± 26	nm

Particle sizes include 95% confidence interval, except that measured via USANS, which references the standard deviation

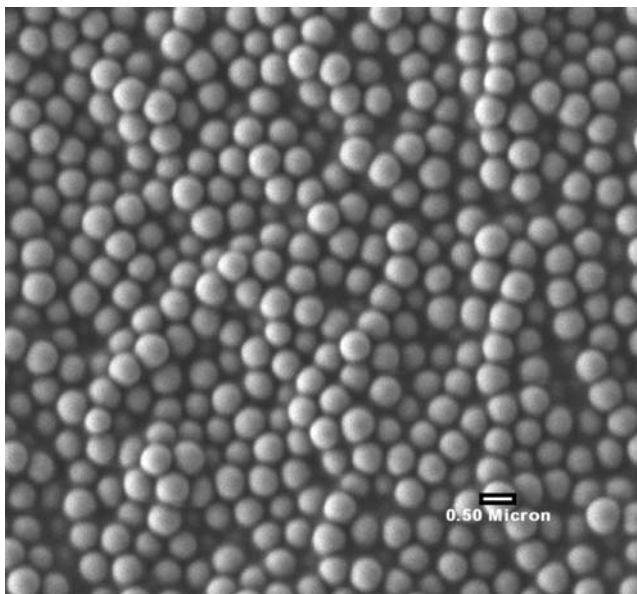


Fig. 1 SEM micrograph of silica particles

be spherical, dispersed in solution, and polydisperse in size.

The surface charge (Maranzano et al. 2000) was probed with a highly sensitive Zeta-PALS instrument (Brookhaven), using ethylene glycol to lower the solvent viscosity and enhance sensitivity. The electrophoretic mobility was below measurement detection and can be assumed to be below $10^{-11} \text{ m}^2 \cdot \text{V}^{-1} \text{ s}^{-1}$ (McNeil-Watson et al. 1998).

Rheological testing

Shear rheology was measured on a stress rheometer (TA Instruments AR-G2, 40 mm 1° aluminum cone and peltier plate at $25 \pm 0.1^\circ \text{C}$). The samples were presheared to remove any loading history by a continuous stress ramp from 0.01 Pa to 1,000 Pa for 3 min for the two lower concentration samples and from 0.1 to 1,500 Pa for the highest concentration sample. After the preshear, the time to achieve steady state was ascertained by shearing at low stresses. (0.01 Pa and 0.1 Pa were applied for 2 min each for the two lowest concentrations; the concentrated sample was sheared at 0.1 and 1 Pa.) Finally, steady-state stress sweeps from 0.01 to 800 Pa, 0.01 to 1,000 Pa, and 0.1 to 1,500 Pa were performed for the $\phi = 0.194, 0.391, \text{ and } 0.490$ samples, respectively. The constant stress tests were repeated, and then steady state sweeps from high to low stress over the same stress range were performed to measure hysteresis or sample degradation. All samples were stable and reversible with negligible hysteresis.

USANS measurements

USANS experiments were performed using the BT5 thermal neutron double-crystal instrument at the National Institute of Standards and Technology (NIST), National Center for Neutron Research (NCNR) in Gaithersburg, MD (Barker et al. 2005; Kim and Glinka 2006). The USANS instrument uses multiple reflections from perfect crystals both to tightly collimate the neutron beam before the sample and select a small wavelength range to be detected on the line detector after the sample. This geometry gives no measure of flow-induced anisotropy. USANS measurements on quiescent samples were performed in 1-mm-thick titanium sandwich cells with quartz windows, except for the highest concentration sample, which was measured in the shear cell due to loading issues in the sandwich cell. The data as recorded has both wavelength smearing ($\lambda = 2.38 \text{ \AA}$, $\Delta\lambda/\lambda = 5.9\%$ wavelength spread) and effective slit smearing (due to the low vertical resolution). The slit smearing dominates, and so, only slit-smearing will be applied to models to fit to the data (Kline 2006).

Here, we also perform the first reported flow-USANS measurements by inserting as the sample geometry the NIST-SANS shear cell (Maranzano et al. 2000; Straty et al. 1991). This sample geometry is a Couette cell with a 60-mm inner quartz cylinder and a 61-mm outer quartz cup driven by a servomotor. The beam is oriented radially through the center of the Couette along the velocity gradient direction and therefore passes through the sample twice. The scattering is a projection in the velocity–vorticity (1–3) plane. The data were reduced using standard procedures (Kline 2006). As noted, USANS yields slit smeared data; hence, under shear, USANS yields a one-dimensional scattering profile that is a slit-smeared average over an anisotropic scattering pattern in the velocity–vorticity (1–3) plane of flow. Therefore, presently, it is not possible to desmear data acquired under flow.

Scattering modeling and analysis

Scattering data from monodisperse scatterers, in terms of absolute scattered intensity (I) versus scattering vector (\mathbf{q}), is described by

$$I(\mathbf{q}, \dot{\gamma}) = A * P(\mathbf{q}, a) * S(\mathbf{q}, a, \phi, \dot{\gamma}) + B, \quad (1)$$

where A is a concentration dependent prefactor; $S(\mathbf{q}, a, \phi, \dot{\gamma})$ is the structure factor, a function of volume fraction, particle size, and particle interactions in the static case but also a function of shear rate (or stress) and, possibly, the flow history; $P(\mathbf{q}, a)$ is the

particle form factor, a function of the particle shape and size; and B is the background scattering, assumed here to be just the incoherent scattering expected based on sample chemistry. The prefactor A is given by Eq. 2:

$$A = n_p V_p^2 (\Delta\rho)^2 = \phi V_p (\Delta\rho)^2, \quad (2)$$

where n_p is the number of particles per unit volume, V_p is the volume of a particle, and $\Delta\rho$ is the difference in scattering length densities (SLD) of the particle and solution. The particle form factor $P(\mathbf{q}, a)$ for a sphere is isotropic and is given by Eq. 3:

$$P(\mathbf{q}, a) = \left[\frac{3(\sin(\mathbf{q}a) - \mathbf{q}a \cos(\mathbf{q}a))}{(\mathbf{q}a)^3} \right]^2. \quad (3)$$

The static structure factor is given by Eq. 4 as the Fourier transform of the radial distribution function, $g(\mathbf{r})$:

$$S(\mathbf{q}) = 1 + n \int [g(\mathbf{r}) - 1] e^{-i\mathbf{q}\cdot\mathbf{r}} d\mathbf{r}, \quad (4)$$

which will be isotropic at rest but can be anisotropic under flow even for spherical particles (Maranzano and Wagner 2002). In the limiting case, as $\phi \rightarrow 0$, $S(\mathbf{q}, \phi \rightarrow 0) = 1$.

The USANS data as collected is slit-smearred. The correction for smearing is given by Eq. 5 under the assumption of isotropic scattering,

$$I_s(\mathbf{q}) = \frac{1}{\Delta\mathbf{q}_v} \int_0^{\Delta\mathbf{q}_v} I(\sqrt{\mathbf{q}^2 + u^2}) du, \quad (5)$$

where I_s is the smeared intensity and $\Delta\mathbf{q}_v$ is the maximum extent of the vertical resolution in the instrument (Kline 2006). When comparing USANS and SANS data, it is important to note that the instrumental smearing of the model in the USANS experiment causes the $I(\mathbf{q} = 0)$ in a USANS measurement [where $P(\mathbf{q} = 0) = 1$] to decrease substantially due to resolution smearing, and is given by Eq. 6:

$$I_s(\mathbf{q} = 0) = \frac{\sqrt{3\pi}\phi V_p (\Delta\rho)^2 * S(\mathbf{q} = 0, a, \phi)}{(2R_g \Delta\mathbf{q}_v)} + B, \quad (6)$$

where R_g is the radius of gyration of the scattering body.

The form factor was determined from a dilute, static measurement ($\phi = 0.01$) and by fitting to the model for a sphere (Eq. 3) that is integrated over a Schulz size distribution (Schulz et al. 1962) and smeared for instrument resolution (Eq. 5).

$$I(\mathbf{q}, \phi = 0.01, \dot{\gamma} = 0) = \phi V_p (\Delta\rho)^2 * \overline{P(\mathbf{q}, a, \sigma)} + B(\phi = 0.01), \quad (7)$$

where the average radius a and polydispersity σ are the fit parameters and $V_p = \frac{4\pi a^3}{3}$. The volume fraction is calculated from the measured densities and weights of addition, and the SLD is allowed to vary only slightly ($\sim 10\%$) from the calculated value.

For concentrated samples at rest, a polydisperse core-shell, hard-sphere structure factor is used for $S(\mathbf{q}, a, \phi)$, where the core size is taken as the radius determined from the form factor, and a thin shell thickness is allowed to compensate for the surface stabilizing layer on the particles. The model approximates the effective hard-sphere structure factor equivalent to the multicomponent expression by using a monodisperse structure factor at an effective sphere diameter and volume fraction to account for polydispersity (see NIST SANS analysis docs or Kline 2006).

For the samples under flow, the data can neither be desmeared, as it is anisotropic, nor can it be forward smeared for comparison with the data as no model exists at present for the anisotropic structure under flow. Therefore, we define an effective structure factor [as is often done for polydisperse systems in SANS (Wagner et al. 1991)] by dividing the measured intensity by the model that is fit to the dilute scattering data, appropriately corrected for the change in particle concentration, as:

$$S^{\text{eff}}(\mathbf{q}, \phi, \dot{\gamma}) = \frac{I(\mathbf{q}, \phi, \dot{\gamma}) - B(\phi)}{I(\mathbf{q}, \phi = 0.01, \dot{\gamma} = 0)_{\text{fit}} - B(\phi = 0.01)} \times \left(\frac{\phi = 0.01}{\phi} \right). \quad (8)$$

Results

Rheological testing

The steady-state shear viscosity measurements are shown in Fig. 2, both in terms of the shear rate and the Peclet number ($Pe = 6\pi\mu a^3/k_b T$). The points marked with drop down lines indicate shear rates at which the USANS scattering measurement was performed. The lowest concentration sample shows only mild shear thinning and thickening, only noticeable on the expanded linear viscosity scale. The higher-concentration samples show significant amounts of shear thinning and thickening. Forward and backward sweeps are shown; the sample has little hysteresis and the shear thickening is reversible. Additional stress jump experiments shown in Fig. 3 indicate that the structural changes are faster than the measurement data acquisition time scale (10 ms) and that the viscosity is steady with time at

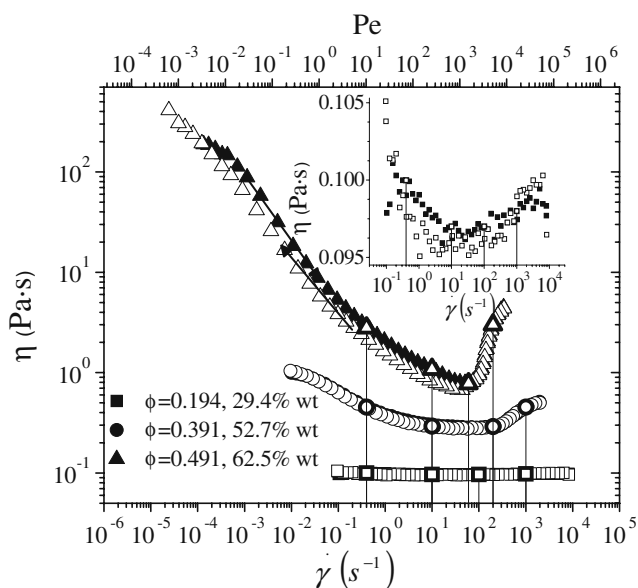


Fig. 2 Steady-shear viscosity of a suspension of silica in PEG. The inset shows an expanded vertical scale for the low-volume fraction sample to show the shear thinning and shear thickening behavior

all shear stresses. These rheological characteristics are consistent with those reported previously for similar, near hard-sphere shear thickening colloidal dispersions (Bender and Wagner 1996; Maranzano and Wagner 2002). The critical values of shear stress, shear rate, and viscosity at the onset of shear thickening (as denoted by the minimum in the viscosity curve) are given in Table 2 along with the suspension concentrations. These values of the critical stress are in good agreement with previously reported values for dispersions of hard spheres (Maranzano and Wagner 2001).

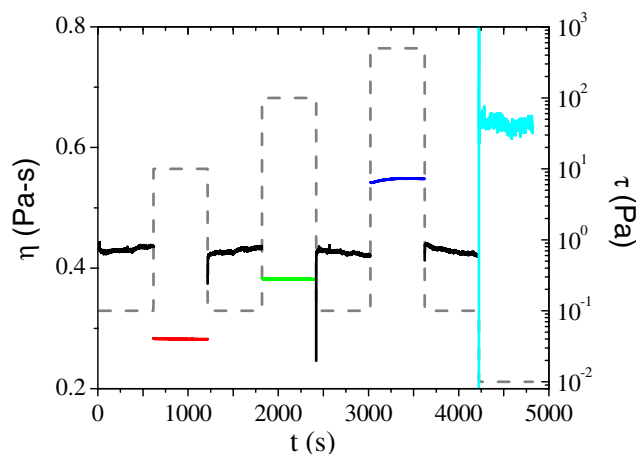


Fig. 3 Stress jump measurements on the $\phi = 0.391$ SiO₂/PEG suspension. The dashed line indicates the applied stress and the solid lines indicate the measured viscosity

Table 2 Suspension properties

ϕ	0.194	0.391	0.490
Solids wt. %	29.4	52.7	62.5
τ_c (Pa)	12.9	63.0	226
η_c (Pa s)	0.0967	0.318	2.99
$\dot{\gamma}_c$ (s ⁻¹)	134	198	75.7

Static USANS

The particle form factor was measured for a dilute sample (Fig. 4) by fitting to Eq. 3 averaged over a Schulz distribution with $\sigma/a = 10\%$. The best fit yielded a radius of 260 nm, in good agreement with SEM measurements (Table 1). The SLD difference used in the fit of $\Delta\rho = 2.06 \times 10^{-6} \text{ \AA}^{-2}$ compares well with the calculated value of $2.57 \times 10^{-6} \text{ \AA}^{-2}$, which assumes the particles as pure SiO₂ and the PEG as pure C₈O₅H₁₈, ignoring any surface stabilizer, particle impurities, solvent impurities (including polydispersity in the PEG molecular weight), or porosity of the particles.

Static USANS measurements of the concentrated samples are shown in Fig. 5 along with fits to the core-shell hard-sphere model, appropriately smeared. The assumption of a shell with no contrast from the solvent was used to account for any surface stabilizers, as well as any other repulsive interparticle interactions. Neither a normal hard-sphere structure factor nor a structure factor based on any simple potential such as the sticky hard-sphere or square-well potential was able to satisfactorily fit these data. In the fitting, the radius and polydispersity determined from the fit of the dilute sample were used. The shell thickness and sphere core SLD were adjusted to give the best fit and the parameters given in Table 3. A good fit is

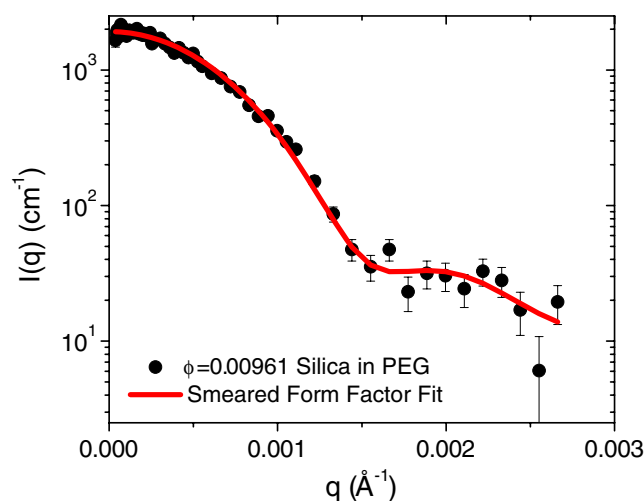


Fig. 4 USANS form factor fit of dilute particle suspension

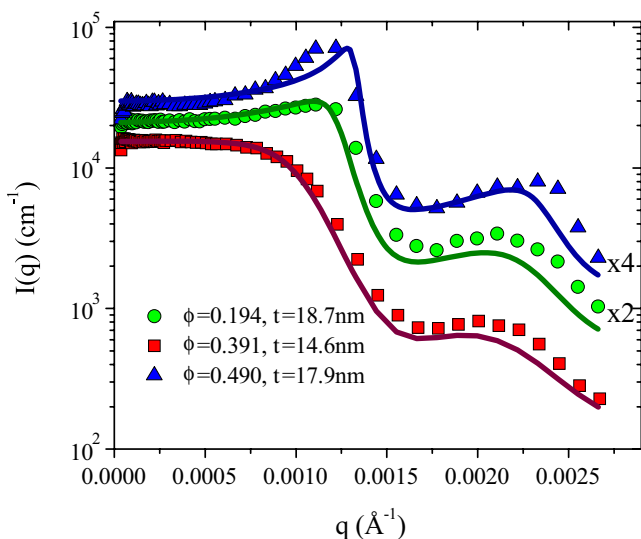


Fig. 5 Static USANS measurements of SiO₂/PEG suspension with core-shell fits (*lines*). The data are shifted as denoted for clarity of presentation

achieved for the two lowest volume fractions. At the highest volume fractions, the effective suspension volume fraction (Table 3) accounting for the shell is well above the volume fraction where hard spheres crystallize (55 vol%) (Pusey and Vanmegen 1986). The data show evidence for a Debye–Shearer peak from a polydisperse crystalline order that is at lower q than would be predicted for a liquid-like order, which is consistent with a polycrystalline structure having, on average, greater nearest neighbor separation than a liquid at the same packing fraction. The sample’s 10% polydispersity is just slightly lower than would be expected to prevent crystallization (Pusey and Vanmegen 1986). This evidence of crystalline order is consistent with the shear viscosity exhibiting evidence of a yield stress (Fig. 2) rather than a finite zero shear viscosity.

USANS transmission measurements

Two transmission measurements are taken in a USANS experiment. One measurement is the ratio of the intensity at zero angle, in the center of the rocking curve, of the sample compared to the empty cell, or T_{rock} . The other measurement is at a large angle, T_{wide} , which

Table 3 Parameters from USANS fitting

	0.194	0.391	0.490
ϕ_{calc}	0.194	0.391	0.490
ϕ_{eff}	0.24	0.46	0.60
$\rho(\text{SLD, SiO}_2) \times 10^6 \text{ \AA}^{-2}$	2.88	2.76	2.86
$\rho(\text{SLD, PEG/shell}) \times 10^6 \text{ \AA}^{-2}$	0.517	0.517	0.517
Shell thickness (nm)	18.7	14.6	17.9

measures transmission from all small-angle scattering (Barker et al. 2005). The ratio of the two, $T_{\text{rock}}/T_{\text{wide}}$, is the fraction of the beam that undergoes small-angle scattering; multiple scattering can be ignored if this ratio is less than 0.9 (Schelten and Schmatz 1980). The measured transmission, seen in Table 4, varied from 0.843 to 0.899, indicating only a small amount of multiple scattering in measurements, and therefore, no further corrections are applied to the data. Also, note that this ratio does not vary substantially or systematically with shear rate, indicating that the integrity of the sample is maintained during the flow-USANS experiments.

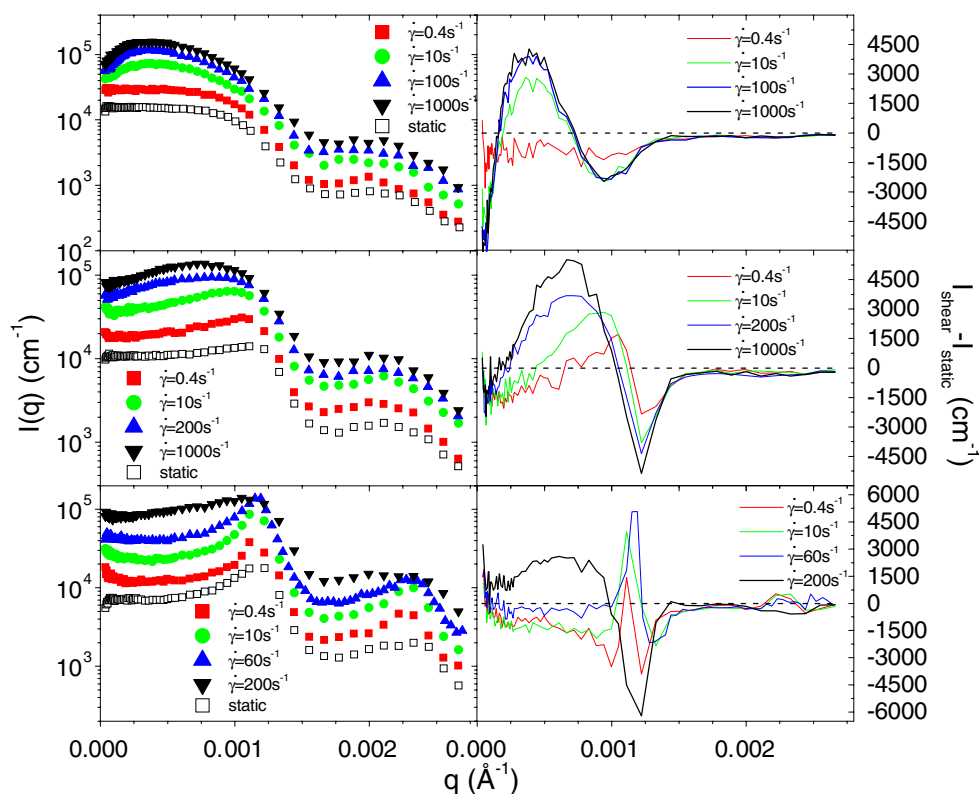
Flow-USANS measurements

USANS measurements taken under steady shear at four shear rates for each of the three concentrated suspensions are shown in Fig. 6, which includes the data collected under static conditions for comparison (Fig. 5). The scattering data collected with the sample under shear are shifted vertically by progressive factors of two for clarity of presentation. The predominant new feature evident in measured intensity under shear is the shift of the scattering peak to lower scattering vector magnitudes, especially for high shear rates in the shear thickening regime. For the lowest concentration sample, the development of a very broad correlation peak at $q \sim 4 \times 10^{-3} \text{ \AA}^{-1}$ is evident with increasing shear. The moderate concentration sample exhibits a scattering peak at rest that increases in magnitude and then broadens and shifts to lower wave vector with increasing shear rate. The high concentration sample shows a sharp peak indicating order or crystallinity upon shearing, which melts into a broad shoulder at

Table 4 Transmission measurements from USANS experiments

ϕ	Shear rate (s ⁻¹)	T_{wide}	T_{rock}	T
0.194	0.4	0.702	0.616	0.877
0.194	10	0.701	0.602	0.859
0.194	100	0.702	0.604	0.860
0.194	1,000	0.699	0.598	0.856
0.391	0.4	0.739	0.634	0.858
0.391	10	0.739	0.623	0.843
0.391	200	0.736	0.621	0.844
0.391	1,000	0.734	0.620	0.845
0.490	0.4	0.760	0.656	0.864
0.490	10	0.759	0.646	0.852
0.490	60	0.757	0.643	0.850
0.490	200	0.757	0.646	0.853
0.194	Static cell	0.731	0.657	0.899
0.391	Static cell	0.759	0.662	0.873
0.491	0	0.784	0.694	0.885

Fig. 6 Flow-USANS measurements for low ($\phi = 0.194$, *top*), moderate ($\phi = 0.391$, *middle*), and high ($\phi = 0.490$, *bottom*) concentration suspensions of SiO₂ in PEG. *Left:* $I(\mathbf{q})$ data under static conditions and at each shear rate, shifted by 2 \times , 4 \times , 6 \times , and 8 \times in order. *Right:* $I(\mathbf{q})$ data under shear subtracted from rest [$I(\mathbf{q})_{\text{static}}$]



low \mathbf{q} at the highest shear rate in the shear thickening regime. These results are similar to prior observations using SANS (Bender and Wagner 1995, 1996; Maranzano and Wagner 2002; Watanabe et al. 1998), but these USANS measurements extend the range of observation to sufficiently low scattering vectors to capture the microstructure in the hydrocluster state at length scales sufficiently larger than the nearest neighbor distances.

To better elucidate the shear-induced structural changes, the right panels in Fig. 6 show the subtraction of the intensity under shear minus that at rest. For the lowest concentration, increasing shear flow leads to the development of a strong, broad correlation peak at $\mathbf{q} \sim 4 \times 10^{-4} \text{ \AA}^{-1}$. This is indicative of cluster formation (Stradner et al. 2004), with a characteristic length scale given by $L \sim 2\pi/\mathbf{q}_{\text{max}} \sim 1,500 \text{ nm}$, or about three particle diameters. Note that this is not a fractal-like or porous structure forming, as it is a clear peak in the scattering and not simply increased forward scattering. The minimum at higher \mathbf{q} is due to a reduction in the equilibrium correlation peak in the structure factor, which is very weak at these low concentrations. Note that hydrocluster formation precedes the actual rise in the overall viscosity as the viscosity is comprised of a shear thinning component due to interparticle forces and a hydrodynamic component sensitive to

the hydrocluster formation (Bender and Wagner 1995; Dhaene et al. 1993). The onset of shear thickening of the hydrodynamic component occurs before the visible rise in the total viscosity (Bender and Wagner 1995; Bergenholtz et al. 2002; Gopalakrishnan and Zukoski 2004). Similar results are observed for the medium concentration dispersion, but this loss in the equilibrium structure correlation peak is more evident as the peak shifts and broadens to lower \mathbf{q} progressively with increasing shear rate. Further, the peak positions are located at higher \mathbf{q} than for the lowest concentration sample due to increased particle concentration. A qualitative difference in behavior is observed for the most concentrated sample, where shearing greatly enhances the Bragg peak evident at equilibrium, which is consistent with shear-induced alignment of polycrystalline samples (Chen et al. 1994). Further shearing leads to shear thickening, which is accompanied by a loss in order (large negative peak) and the formation of a cluster peak that is qualitatively similar to that observed for the lower two concentrations, but broader and lower in magnitude.

Attempts were made to develop real-space models to fit these complex structure factors under flow, but no successful, physically meaningful fits were achieved. This is most likely due to the highly anisotropic nature of the scattering at high shear rates (Laun et al.

1992; Lee and Wagner 2006; Maranzano and Wagner 2002; Newstein et al. 1999; Watanabe et al. 1998); slit smearing; and, possibly, multiple scattering. Therefore, we proceed to further analyze and discuss the results through the effective structure factors as defined in Eq. 8.

The measured effective (smeared) structure factors for the samples at rest are shown in Fig. 7. Also included in Fig. 7 is the calculated effective polydisperse hard sphere structure factor; this calculated structure factor is the same structure factor used in Fig. 5, combined with the particle form factor and instrumental smearing. Note that, as discussed in the “Experimental” section, the measured effective structure factors will only equal the actual structure factor if there are no effects of instrument smearing, anisotropy, size polydispersity, or multiple scattering—hence, the quantitative differences with the true structure factors shown for reference in Fig. 7. Nonetheless, this comparison shows the features of these effective structure factors qualitatively represent those of the true, underlying structure. Also shown is the form factor, where the first form factor minima is observed to fall just beyond the first peak in the scattering and, therefore, does not interfere with the observations of how that peak shifts under shear flow.

Figure 8 shows the effective structure factors under flow, which look similar in form to those at rest but evolve systematically with applied shear rates. With increasing shear rate, the nearest neighbor peak shifts to higher q , indicating particles moving closer together, while a broad shoulder develops at lower q . To better illustrate the shear-induced microstructural changes, the right panel of Fig. 8 shows the corresponding differences as the subtraction of these effective structure factors under flow minus the static values. Two features are clearly evident in the lowest concentration sample: flow enhances the structure peak corresponding to the

nearest neighbor correlations, and high shear rates lead to the growth of a broad peak centered around $q_c^* \sim 4 \times 10^{-4} \text{ \AA}^{-1}$. This new peak not evident in the equilibrium structures indicates clusters with a characteristic cluster separation distance of $2\pi/q_c^* \sim 1,500 \text{ nm}$ (Groenewold and Kegel 2001; Stradner et al. 2004). The second, sharper peak, centered on $q_m^* \sim 1.4 \times 10^{-3} \text{ \AA}^{-1}$, indicates the interparticle separation distance within a cluster of $2\pi/q_m^* \sim 450 \text{ nm}$, slightly smaller than the diameter of a particle, indicating that the particles are nearly close-packed (note, this value is approximate partly due to the smearing effects present in the effective structure factor). For the lowest concentration, $\phi = 0.194$ sample, the higher q peak (nearest neighbor correlation) appears already at the lowest shear rate, but the cluster peak does not appear until 10 s^{-1} , at which point there is little change up to a shear rate of $1,000 \text{ s}^{-1}$. Note that the shear viscosity is thinning at the lowest measured shear rate (0.4 s^{-1}) and only weakly shear thickening for the three higher shear rates ($10, 10^2, 10^3 \text{ s}^{-1}$). Also, at this concentration, the peak locations do not change with shear rate. Finally, large rearrangements are evident at this lower volume fraction in part because there is substantial free volume available to accommodate restructuring of the microstructure by flow.

At moderate concentration of $\phi = 0.391$, a similar effect is observed, where the first peak in the structure factor broadens with increasing shear rate. This leads to a splitting in the subtracted pattern, as particle correlations strengthen at both lower q (cluster peak) and at higher q (close packing) relative to the liquid correlation peak at rest. Note that the structure factor at this concentration and low q is very low, and so, the magnitude of the cluster peak is small; the changes are more evident when examining the intensity directly (Fig. 6). At the lowest shear rate, in the shear thinning regime, the primary difference is an increase in

Fig. 7 Particle form factor and measured effective smeared structure factors (left panel, shifted as indicated for clarity) under static conditions. The right panel shows the calculated effective structure factors (note—not smeared) for reference

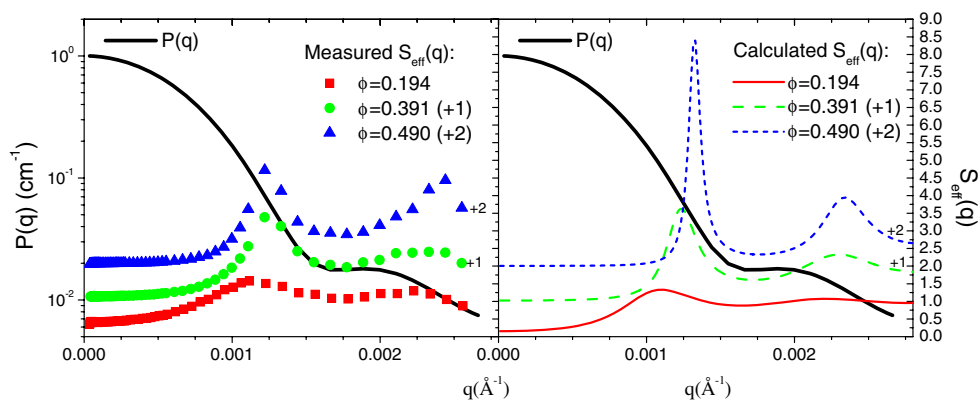
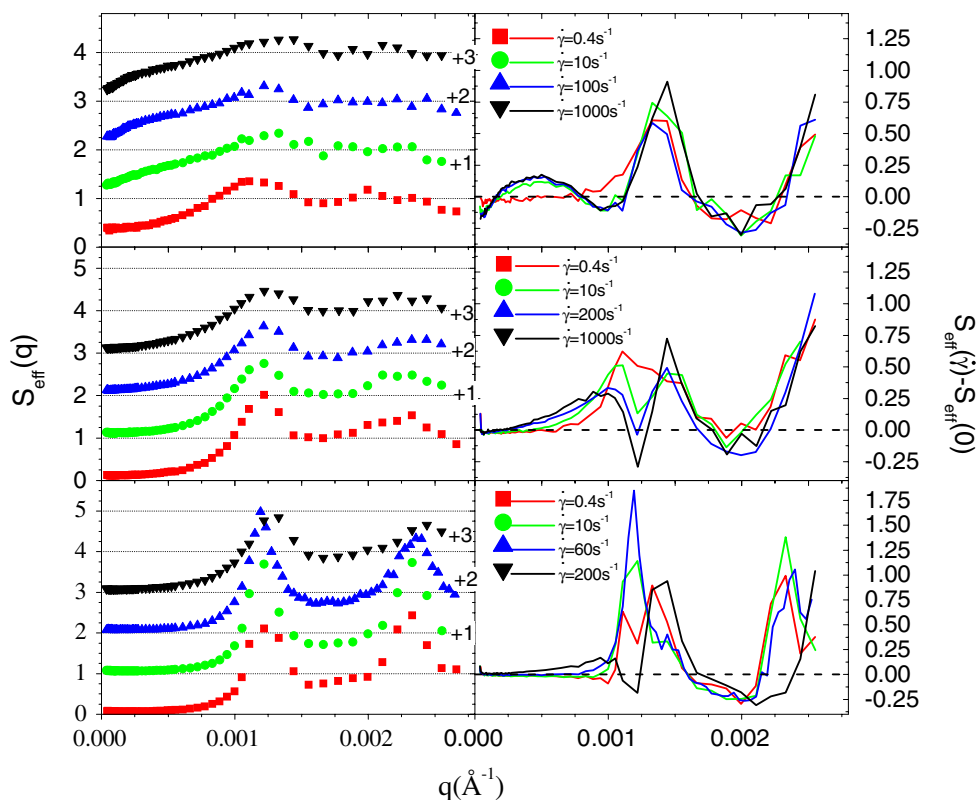


Fig. 8 *Left:* Effective steady-shear structure factors measured via USANS on low ($\phi = 0.194$, *top*), moderate ($\phi = 0.391$, *middle*), and high ($\phi = 0.490$, *bottom*) concentration suspensions of SiO₂ in PEG. Data progress from rest to high shear rates vertically and are shifted vertically with increasing shear rate for clarity. *Right:* Static structure factor with equilibrium structure factor subtracted to show growth of cluster peaks



the magnitude of the correlation peak compared to static conditions. At the three highest shear rates, the viscosity reaches an intermediate shear plateau before gradually shear thickening. In this regime, a cluster peak forms with the associated shift of the nearest neighbor peak toward close packing. The magnitude of the restructuring under flow is less than that observed at the lower volume fraction as the fluid is concentrated, so there is substantially less free volume available for restructuring. Nonetheless, relatively small changes in microstructure can have substantial quantitative effects on the shear viscosity at these high concentrations.

Finally, for the most concentrated sample, the primary peak corresponds to a first-order Bragg peak for a closely packed structure at an effective volume fraction of ~ 0.6 . This peak continues to sharpen and grow with increasing shear rates, while the viscosity shows shear thinning. Only at the highest shear rate, which shows substantial shear thickening, does the sample exhibit the traits observed for the liquid samples described previously, namely, the formation of a cluster peak at low q and the commensurate enhancement of scattering intensity corresponding to a closely packed neighbor correlation. Ordering of the suspension into shear planes, observed via these measurements, leads to a lower viscosity fluid (Rastogi et al. 1996), whereas the hydroclustering seen at higher shear rates leads to a

substantial increase in the hydrodynamic component of the viscosity (Brady and Bossis 1988; Brady and Morris 1997; Laun et al. 1992; Maranzano and Wagner 2001).

We also observe evidence for the loss of order upon shear thickening from a flowing, crystalline suspension as originally proposed by Hoffman (Hoffman 1972). The mechanism for flow destabilization proposed by Hoffmann is hydrodynamic in origin (i.e., neighboring particles coupling hydrodynamically due to fluctuations in position, leading to doublet rotation out of the flowing shear planes and disruption of the stratified flow). However, the mechanism of returning to a liquid-like structure under flow is insufficient to explain the magnitude of the increase in viscosity upon shear thickening (Laun et al. 1991) (although, see Hoffman 1998 for a differing viewpoint). The measurements here, however, show that the large increase in stress is accompanied by the formation of hydroclusters (Bender and Wagner 1995; Bossis and Brady 1989; Brady and Bossis 1988; Brady and Morris 1997; Dhaene et al. 1993; Maranzano et al. 2000; Melrose et al. 1996; Newstein et al. 1999; O'Brien and Mackay 2000; Phung et al. 1996; Watanabe et al. 1998), a microstructure with correlated density fluctuations that is distinctly different from that for a flowing liquid. Indeed, previous measurements have demonstrated a quantitative correlation between the hydroclustered microstructure of the shear thickened

state and the shear rheology (Maranzano and Wagner 2002).

These USANS measurements show that reversible shear thickening is accompanied by correlated density fluctuations, denoted as hydroclusters, and that these hydroclusters are of finite extent and are comprised of fluctuations of closely packed particles. These results are in good qualitative agreement with simulations of flowing suspensions that include hydrodynamic interactions (Bossis and Brady 1989; Brady and Bossis 1988; Brady and Morris 1997; Catherall et al. 2000; Melrose and Ball 2004; Melrose et al. 1996; Phung et al. 1996), and are consistent with prior experimental measurements showing structural changes on the length scale of the nearest neighbor correlations upon shear thickening. The new results, however, are an explicit demonstration of a cluster peak in the hydroclustered state, suggesting that hydroclusters are of finite extent and are highly correlated.

Finally, although USANS provides new and valuable evidence for the time-averaged structure of the hydroclustered state, the technique is limited in that it cannot provide information about the temporal nature of the fluctuations that are sometimes observed in shear thickening dispersions near the jamming transition (Lootens et al. 2003). Furthermore, unlike prior work, where a quantitative 3-D reconstruction of the shear-thickened microstructure enabled quantitatively connecting the microstructure to the hydrodynamic and thermodynamic stresses (Maranzano and Wagner 2002; Wagner and Ackerson 1992), the 1-D averaging of the USANS spectra prevents us from performing a similar quantitative analysis. Nonetheless, these results demonstrate that new correlations arise in hydroclustered colloidal suspensions. A new sample environment developed for SANS now enables measurements in the 1–2 plane of shear (Liberatore et al. 2006). Future studies will be performed with this instrumentation to resolve the structure of hydroclusters in the plane of shear.

Conclusions

Flow-USANS measurements under flow have been conducted for the first time to study the restructuring of the colloidal microstructure during shear thinning and shear thickening on length scales sufficient to elucidate the formation of hydroclusters. These observations provide direct evidence for the formation of hydroclusters in stable, near hard-sphere colloidal suspensions at high Peclet numbers. Further, we find the hydroclusters to be correlated density fluctuations of finite spatial extent in a shear thickening colloidal suspension. The hydro-

clusters are essentially close-packed. The breadth of the scattering cluster peak suggests a broad size range for these fluctuations, but a more detailed analysis is not possible given the instrument limitations of slit smearing anisotropic structures. The structural measurements confirm expectations that hydroclusters are fluctuations in the form of transient, compact clusters as opposed to large, cell-spanning, fractal-like aggregates. In addition, the measurements compare well with prior optical and SANS measurements, as well as simulation and theory showing that the hydrocluster formation precedes the rise in measured viscosity. We also demonstrate, in agreement with prior work, that an order–disorder transition may accompany shear thickening, but that it is not necessary for shear thickening, and that the shear-thickened state after shear melting is marked by the presence of hydroclusters.

Acknowledgements Research was sponsored by the US Army Research Office and the US Army Research Laboratory and was accomplished under Cooperative Agreement Number W911NF-05-2-0006. The views and conclusions contained in this document are those of the authors and should not be interpreted as representing the official policies, either expressed or implied, of the Army Research office, the Army Research Laboratory, or the US Government. The US Government is authorized to reproduce and distribute reprints for Government purposes notwithstanding any copyright notation hereon. This work utilized facilities supported in part by the National Science Foundation under Agreement No. DMR-0454672. We acknowledge the support of the National Institute of Standards and Technology, US Department of Commerce, in providing the neutron research facilities used in this work, as well as the assistance of Lionel Porcar and Man-Ho Kim. The authors thank Prof. Peter Schurtenberger (Uni. Fribourg) for helpful discussions about the cluster peak.

References

- Ackerson BJ, Hayter JB, Clark NA et al (1986) Neutron scattering from charge stabilized suspensions undergoing shear. *J Chem Phys* 84:2344–2349
- Ackerson BJ, Dekruif CG, Wagner NJ et al (1989) Comparison of small shear-flow rate small wave vector static structure factor data with theory. *J Chem Phys* 90:3250–3253
- Barker JG, Glinka CJ, Moyer JJ et al (2005) Design and performance of a thermal-neutron double-crystal diffractometer for USANS at NIST. *J Appl Crystallogr* 38:1004–1011
- Barnes HA (1989) Shear-thickening (Dilatancy) in suspensions of nonaggregating solid particles dispersed in Newtonian liquids. *J Rheol* 33:329–366
- Bender JW, Wagner NJ (1995) Optical measurement of the contributions of colloidal forces to the rheology of concentrated suspensions. *J Colloid Interface Sci* 172:171–184
- Bender J, Wagner NJ (1996) Reversible shear thickening in monodisperse and bidisperse colloidal dispersions. *J Rheol* 40:899–916
- Bergenholtz J, Brady JF, Vicic M (2002) The non-Newtonian rheology of dilute colloidal suspensions. *J Fluid Mech* 456: 239–275

- Bhatia SR (2005) Ultra-small-angle scattering studies of complex fluids. *Curr Opin Colloid Interface Sci* 9:404–411
- Bossis G, Brady JF (1989) The rheology of Brownian suspensions. *J Chem Phys* 91:1866–1874
- Brady JF (1996) Model hard-sphere dispersions: statistical mechanical theory, simulations, and experiments. *Curr Opin Colloid Interface Sci* 1:472–480
- Brady JF, Bossis G (1985) The rheology of concentrated suspensions of spheres in simple shear-flow by numerical-simulation. *J Fluid Mech* 155:105–129
- Brady JF, Bossis G (1988) Stokesian dynamics. *Annu Rev Fluid Mech* 20:111–157
- Brady JF, Morris JF (1997) Microstructure of strongly sheared suspensions and its impact on rheology and diffusion. *J Fluid Mech* 348:103–139
- Catherall AA, Melrose JR, Ball RC (2000) Shear thickening and order–disorder effects in concentrated colloids at high shear rates. *J Rheol* 44:1–25
- Chen LB, Chow MK, Ackerson BJ et al (1994) Rheological and microstructural transitions in colloidal crystals. *Langmuir* 10:2817–2829
- Decker MJ, Halbach CJ, Nam CH et al (2007) Stab resistance of shear thickening fluid (STF)-treated fabrics. *Compos Sci Technol* 67:565–578
- Dekruif CG, Briels WJ, May RP et al (1988) Hard-sphere colloidal silica dispersions—the structure factor determined with sans. *Langmuir* 4:668–676
- Dhaene P, Mewis J, Fuller GG (1993) Scattering dichroism measurements of flow-induced structure of a shear thickening suspension. *J Colloid Interface Sci* 156:350–358
- Fischer C, Plummer CJG, Michaud V et al (2007) Pre- and post-transition behavior of shear-thickening fluids in oscillating shear. *Rheol Acta* 46:1099–1108
- Gopalakrishnan V, Zukoski CF (2004) Effect of attractions on shear thickening in dense suspensions. *J Rheol* 48:1321–1344
- Groenewold J, Kegel WK (2001) Anomalously large equilibrium clusters of colloids. *J Phys Chem B* 105:11702–11709
- Hoekstra H, Vermant J, Mewis J et al (2002) Rheology and structure of suspensions in liquid crystalline hydroxypropyl-cellulose solutions. *Langmuir* 18:5695–5703
- Hoekstra H, Mewis J, Narayanan T et al (2005) Multi length scale analysis of the microstructure in sticky sphere dispersions during shear flow. *Langmuir* 21:11017–11025
- Hoffman RL (1972) Discontinuous and dilatant viscosity behavior in concentrated suspensions. I. Observation of a flow instability. *Trans Soc Rheol* 16:155–173
- Hoffman RL (1998) Explanations for the cause of shear thickening in concentrated colloidal suspensions. *J Rheol* 42:111–123
- Johnson SJ, Dekruif CG, May RP (1988) Structure factor distortion for hard-sphere dispersions subjected to weak shear-flow—small-angle neutron-scattering in the flow-vorticity plane. *J Chem Phys* 89:5909–5921
- Kim MH, Glinka CJ (2006) Ultra small angle neutron scattering study of the nanometer to micrometer structure of porous Vycor. *Microporous Mesoporous Mater* 91:305–311
- Kline SR (2006) Reduction and analysis of SANS and USANS data using IGOR Pro. *J Appl Crystallogr* 39:895–900
- Krishnamurthy LN, Wagner NJ, Mewis J (2005) Shear thickening in polymer stabilized colloidal dispersions. *J Rheol* 49:1347–1360
- Laun HM, Bung R, Schmidt F (1991) Rheology of extremely shear thickening polymer dispersions (Passively Viscosity Switching Fluids). *J Rheol* 35:999–1034
- Laun HM, Bung R, Hess S et al (1992) Rheological and small-angle neutron-scattering investigation of shear-induced particle structures of concentrated polymer dispersions submitted to plane poiseuille and couette-flow. *J Rheol* 36:743–787
- Lee YS, Wagner NJ (2006) Rheological properties and small-angle neutron scattering of a shear thickening, nanoparticle dispersion at high shear rates. *Ind Eng Chem Res* 45:7015–7024
- Lee YS, Wetzel ED, Wagner NJ (2003) The ballistic impact characteristics of Kevlar (R) woven fabrics impregnated with a colloidal shear thickening fluid. *J Mater Sci* 38:2825–2833
- Liberatore MW, Nettekheim F, Wagner NJ et al (2006) Spatially resolved small-angle neutron scattering in the 1–2 plane: a study of shear-induced phase-separating wormlike micelles. *Phys Rev E* 73:020504–020501–020504
- Lindner P, Oberthur RC (1984) Apparatus for the investigation of liquid-systems in a shear gradient by small-angle neutron-scattering (SANS). *Rev Phys Appl* 19:759–763
- Lootens D, Van Damme H, Hebraud P (2003) Giant stress fluctuations at the jamming transition. *Phys Rev Lett* 90:178301
- Lootens D, Hebraud P, Lecolier E et al (2004) Gelation, shear-thinning and shear-thickening in cement slurries. *Oil Gas Sci Technol Rev Inst Fr Pet* 59:31–40
- Maranzano BJ, Wagner NJ (2001) The effects of interparticle interactions and particle size on reversible shear thickening: hard-sphere colloidal dispersions. *J Rheol* 45:1205–1222
- Maranzano BJ, Wagner NJ (2002) Flow-small angle neutron scattering measurements of colloidal dispersion microstructure evolution through the shear thickening transition. *J Chem Phys* 117:10291–10302
- Maranzano BJ, Wagner NJ, Fritz G et al (2000) Surface charge of 3-(trimethoxysilyl) propyl methacrylate (TPM) coated Stober silica colloids by zeta-phase analysis light scattering and small angle neutron scattering. *Langmuir* 16:10556–10558
- McNeil-Watson F, Tscharnuter W, Miller J (1998) A new instrument for the measurement of very small electrophoretic mobilities using phase analysis light scattering (PALS). *Colloids Surf A Physicochem Eng Asp* 140:53–57
- Melrose JR, Ball RC (2004) Continuous shear thickening transitions in model concentrated colloids—the role of interparticle forces. *J Rheol* 48:937–960
- Melrose JR, vanVliet JH, Ball RC (1996) Continuous shear thickening and colloid surfaces. *Phys Rev Lett* 77:4660–4663
- Newstein MC, Wang H, Balsara NP et al (1999) Microstructural changes in a colloidal liquid in the shear thinning and shear thickening regimes. *J Chem Phys* 111:4827–4838
- O'Brien VT, Mackay ME (2000) Stress components and shear thickening of concentrated hard sphere suspensions. *Langmuir* 16:7931–7938
- Phung TN, Brady JF, Bossis G (1996) Stokesian dynamics simulation of Brownian suspensions. *J Fluid Mech* 313:181–207
- Pusey PN, Vanmegen W (1986) Phase-behavior of concentrated suspensions of nearly hard colloidal spheres. *Nature* 320:340–342
- Rastogi SR, Wagner NJ, Lustig SR (1996) Microstructure and rheology of polydisperse, charged suspensions. *J Chem Phys* 104:9249–9258
- Schelten J, Schmatz W (1980) Multiple-scattering treatment for small-angle scattering problems. *J Appl Crystallogr* 13:385–390
- Schulz GV, Scholz A, Figini RV (1962) Analyse zweier charakteristischer verteilungen von polystyrol durch kolonnenfraktionierung. *Makromol Chem* 57:220–240
- Shenoy SS, Wagner NJ, Bender JW (2003) E-FiRST: electric field responsive shear thickening fluids. *Rheol Acta* 42:287–294

- Stradner A, Sedgwick H, Cardinaux F et al (2004) Equilibrium cluster formation in concentrated protein solutions and colloids. *Nature* 432:492–495
- Straty GC, Hanley HJM, Glinka CJ (1991) Shearing apparatus for neutron-scattering studies on fluids—preliminary-results for colloidal suspensions. *J Stat Phys* 62:1015–1023
- Tomita M, Vandeven TGM (1984) The structure of sheared ordered lattices. *J Colloid Interface Sci* 99:374–386
- Vanderwerff JC, Ackerson BJ, May RP et al (1990) Neutron-scattering from dense colloidal dispersions at high shear rates—the deformation of the structure factor in the shear plane. *Physica A* 165:375–398
- Vermant J, Solomon MJ (2005) Flow-induced structure in colloidal suspensions. *J Phys Condens Matter* 17:R187–R216
- Versmold H, Musa S, Dux C et al (2001) Shear-induced structure in concentrated dispersions: small angle synchrotron X-ray and neutron scattering. *Langmuir* 17:6812–6815
- Versmold H, Dux C, Musa S (2002a) On the structure of charge stabilized polymer dispersions. *J Mol Liq* 98–9:145–162
- Versmold H, Musa S, Bierbaum A (2002b) Concentrated colloidal dispersions: on the relation of rheology with small angle x-ray and neutron scattering. *J Chem Phys* 116:2658–2662
- Versmold H, Musa S, Kubetzki H et al (2005) Stacking structure of concentrated shear ordered dispersions by two scattering methods. *Langmuir* 21:4324–4327
- Wagner NJ, Ackerson BJ (1992) Analysis of nonequilibrium structures of shearing colloidal suspensions. *J Chem Phys* 97:1473–1483
- Wagner NJ, Bender JW (2004) The role of nanoscale forces in colloid dispersion rheology. *MRS Bull* 29:100–106
- Wagner NJ, Russel WB (1990) Light-scattering measurements of a hard-sphere suspension under shear. *Phys Fluids A Fluid Dyn* 2:491–502
- Wagner NJ, Krause R, Rennie AR et al (1991) The microstructure of polydisperse, charged colloidal suspensions by light and neutron-scattering. *J Chem Phys* 95:494–508
- Watanabe H, Yao ML, Osaki K et al (1998) Nonlinear rheology and flow-induced structure in a concentrated spherical silica suspension. *Rheol Acta* 37:1–6
- Woutersen A, May RP, Dekruif CG (1993) The shear-distorted microstructure of adhesive hard-sphere dispersions—a small-angle neutron-scattering study. *J Rheol* 37:71–88